SAND2020-13181C

Nonlinear dynamic analysis of a shape changing finger-like mechanism for morphing wings

Aabhas Singh[1], Kayla M. Wielgus[2], Ignazio Dimino[3], Robert J. Kuether[4], Matthew S. Allen[1]

[1] University of Wisconsin – Madison
Email: **singh36@wisc.edu, matt.allen@wisc.edu**

[2] University of Washington
Email: **kwielgus@uw.edu**

[3] Italian Aerospace Research Center
Email: **L.Dimino@cira.it**

[4] Sandia National Laboratories*
Email: **rjkueth@sandia.gov**

ABSTRACT

Morphing wings have great potential to dramatically improve the efficiency of future generations of aircraft and to reduce noise and emissions. Among many camber morphing wing concepts, shape changing finger-like mechanisms consist of components, such as torsion bars, bushings, bearings, and joints, all of which exhibit damping and stiffness nonlinearities that are dependent on excitation amplitude. These nonlinearities make the dynamic response difficult to model accurately with traditional simulation approaches. As a result, at high excitation levels, linear finite element models may be inaccurate, and a nonlinear modeling approach is required to capture the necessary physics. This work seeks to better understand the influence of nonlinearity on the effective damping and natural frequency of the morphing wing through the use of quasi-static modal analysis and model reduction techniques that employ multi-point constraints (i.e. spider elements). With over 500,000 elements and 39 frictional contact surfaces, this represents one of the most complicated models to which these methods have been applied to date. The results to date are summarized and lessons learned are highlighted.

1.0 INTRODUCTION

A morphing wing has great potential to improve the design and operation of future generations of aircraft. Due to the adaptive nature of the mechanism, the aircraft wing geometry may transform into optimal shapes given the flight condition. Camber morphing technology, for instance, may enhance aircraft high-lift performance during take-off and landing by reducing friction drag and aerodynamic noise. During high speed flight, the last portion of the flap may be also adjusted to reduce the overall aerodynamic drag by reducing fuel consumption and emissions [1], [2], [3]. Among the wide range of aerodynamic benefits, the morphing wing may also suppress the need for flap track fairings used to hide the flap deployment mechanism, with additional benefits on aerodynamic efficiency in cruise. NASA and Boeing adapted this concept to Mission Adaptive Wing F111 program [4], [5] in the 1980's. The F111 morphing wing mechanism allowed the outer wing of the aircraft to flex from high to low camber to adjust to flight conditions, resulting in performance benefits in all flight phases, ranging from 7 to 20 percent reduction in drag [6]. More recently, in 2016 a full-size morphing wing was flight-tested by a consortium made of NASA, US Air Force Research Lab, Gulfstream and FlexSys [7].

* Sandia National Laboratories is a multimission laboratory managed and operated by National Technology and Engineering Solutions of Sandia, LLC., a wholly owned subsidiary of Honeywell International, Inc., for the U.S. Department of Energy's National Nuclear Security Administration under contract DE-NA-0003525.

With the rising interest of utilizing morphing aero-structures, there come several challenges. For instance, the added degrees-of-freedom (DOFs) generate systems with increased modal density, producing a more complex aeroelastic behavior which may lead to flutter instabilities. Two kinds of architectures are currently studied to implement the morphing wing capability based on either compliant or kinematic layouts. Compliant layouts involve the controlled deformation of subcomponents to smoothly modify the overall shape of the assembly [8]–[10]. This involves tailoring the structural stiffness to ensure enough compliance to accommodate large deformations and enough robustness to preserve a given shape under external aerodynamic loads. Likewise, kinematic layouts, also referred to as finger-like mechanism-based morphing structures, target the design of skeleton-like articulations with multi-hinge arrangements to enable shape adaptation of large aircraft lifting surfaces [11]–[13]. More specifically, the inner structure is articulated with different rigid parts moving according to mechanical law; the shape change is obtained through the activation of a mechanism that consists of a load-bearing actuator and a transmission line able to withstand aerodynamic loads. Finally, a morphing external skin envelopes the skeleton to preserve geometrical smoothness during shape changing.

In traditional modeling strategies typically used in the aerospace industry, the morphing wing's individual subsystems and components such as torsion bars, bushings, bearings, and joints are assumed rigid. In simulations, inexpensive rigid connectors may be used to replace fully discretized hinges and bushing to reduce computational costs while globally capturing the macroscopic response. This approach may be valid for relatively simple layouts (as in the case of traditional wing flap systems) but may not be valid for adaptive systems involving several mechanical parts. Nonlinear joints and frictional interfaces cause more complex structures to have nonlinear damping and nonlinear stiffness. These nonlinearities make their behavior difficult to model accurately with traditional simulation approaches. For instance, structures have shown to exhibit amplitude dependent damping and natural frequencies that change with excitation amplitude and may even vary depending on the actual shape or configuration. As a result, when nonlinear effects are present at high excitation force levels, operative response predictions using linear finite element models may be inaccurate and detailed, nonlinear modeling approaches should be developed to capture the necessary physics associated with the joints and interface conditions.

In this work, a single adaptive rib of the morphing trailing edge device developed in the framework of the SARISTU project is considered as benchmark [1], [18],[25]. Inspired by a "finger-like" mechanism, as shown in Fig. 1, this mechanism was already successfully validated on both a full scale morphing wing trailing edge [14, p. 22], [15, p. 23], [16] and aileron demonstrators [17]–[19]. However, for the purposes of this research, the morphing trailing edge mechanism was re-engineered to allow for easier manufacturing and assembly in the absence of the morphing skins and other parts while remaining fully representative of the actual subassembly design. The morphing mechanism consists of four consecutive hinge-connected blocks, referred to as B0, B1, B2, and B3, whose relative rotations enable the trailing edge camber morphing. Block B0 is rigidly connected to a test-fixture, while all other blocks are free to rotate around the hinges on the camber line, thus physically turning the camber line into an articulated chain of consecutive segments. Linking rod elements (L1, L2), hinged on non-adjacent blocks, force the camber line segments to rotate according to a specific gear ratio compliant with the shapes to be achieved. The resulting system is a single-degree-of-freedom (SDOF) architecture; if rotation of any of the blocks is prevented, no change in shape can be obtained. On the contrary, if an actuator moves any of the blocks, all the other blocks follow the movement accordingly.

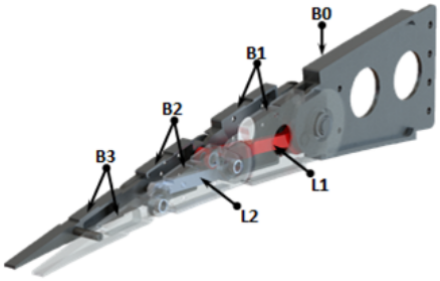

Figure 1: *Example of trailing edge rib mechanism developed in the framework of the SARISTU project [20]*

Due to the large number of joints and contact interfaces involved in the morphing wing design, nonlinearities are associated with friction, clearance, or bilinear stiffness between the pre-loaded contacting surfaces. These nonlinearities introduce variations in the damping ratio and natural frequencies, which are dependent on excitation amplitude. Quasi-static modal analysis (QSMA) [21] can be utilized to extract the amplitude dependent frequency and damping curves from the finite element model using only quasi-static simulations. With this approach, the structure is statically loaded with a force proportional to a vibration mode of interest, and the static response is computed at various load levels. Modal hysteresis loops are then calculated from the load-displacement curves to evaluate the nonlinear behavior of each mode. With over 500,000 elements and 39 frictional contact surfaces in the finite element model, this represents one of the most complicated models to which these methods have been applied to date. Additionally, a reduced order model is developed using the whole joint approach [22] to examine the effect of the rotational spring stiffness on the particular mode of interest.

Section 2 provides a theoretical background of the QSMA approach for nonlinear finite element models. Section 3 discusses modeling efforts on the morphing wing, and Section 4 utilizes QSMA and model reduction techniques in an effort to characterize the frictional nonlinearity in the structure. Section 5 ends with conclusions and a discussion of future work.

2.0 THEORY – QUASI-STATIC MODAL ANALYSIS

To gain insight into the nonlinear behavior of a structure, dynamic transient simulations are able to predict the response to various loading scenarios at different load levels, analogous to simulated experiments. Transient simulations provide data to infer the change of the modal characteristics due to the presence of nonlinearity, but is often too computationally expensive [23] because of the cost associated with time-marching algorithms. Quasi-Static Modal Analysis provides an alternate approach which utilizes quasi-static loading to determine the modal frequency and damping with respect to excitation amplitude. These quantities are obtained at a reduced computational cost relative to transient simulations but are only applicable to models with frictional nonlinearities in microslip. The method used is a variation to the one developed by Festjens et. al. [24] which was extended to whole joint models by Lacayo and Allen [21] and later to nonlinear finite element models in [23]. A brief overview is presented here but the reader is referred to [21], [23] for additional details and limitations.

Consider the equation of motion for a multi degree of freedom system as given by Eq. 1 with $\mathbf{M}$ and $\mathbf{K}$ as the $N \times N$ mass and stiffness matrices, $\boldsymbol{u}$ as the $N \times 1$ displacement vector and the dot notation noting the derivatives with respect to time. $\boldsymbol{F_J}$ and $\boldsymbol{F_{ext}}$ are the $N \times 1$ vectors of frictional contact forces and external applied loads, respectively. The joint force is represented by a model of internal sliders where $\boldsymbol{\theta}$ is a vector to capture the stuck/slip state and the displacement of each slider. It is assumed that the joint forces depend nonlinearly on the displacements.

$$\mathbf{M}\ddot{\boldsymbol{u}} + \mathbf{K}\boldsymbol{u} + \boldsymbol{F_J}(\boldsymbol{u},\boldsymbol{\theta}) = \boldsymbol{F_{ext}} \tag{1}$$

At low amplitudes, the joint force can be linearized by evaluating the derivative of the frictional contact force about the equilibrium position, $\boldsymbol{u_0}$,

$$\mathbf{K}_{\mathrm{T}} = \left.\frac{\partial \boldsymbol{F_J}}{\partial \boldsymbol{u}}\right|_{\boldsymbol{u_0}} \tag{2}$$

The vibration modes are computed about the linearized state (e.g. after applying a preload) by solving the eigenvalue problem where ω_r is the r^{th} natural frequency and $\boldsymbol{\phi}_r$ is the r^{th} mode shape vector,

$$\left(\boldsymbol{K} + \boldsymbol{K}_T - \omega_r^2 \boldsymbol{M}\right)\boldsymbol{\phi}_r = 0 \tag{3}$$

Following the linearized modal analysis, QSMA applies a load in the shape of a mode of interest for incrementing load levels, α, on the static equation of motion as given by

$$\mathbf{K}\boldsymbol{u} + \boldsymbol{F_J}(\boldsymbol{u},\boldsymbol{\theta}) = \boldsymbol{F_{pre}} + \mathbf{M}\boldsymbol{\phi_r}\alpha \tag{4}$$

The $N \times 1$ vector $\boldsymbol{F_{pre}}$ represents the preload force that was used to linearize the system. The static response $\boldsymbol{u}(\alpha)$ can be found by solving Eq. 4 at each load increment, from which the modal amplitude is calculated by using an appropriate modal filter. Next the initial loading curve is computed in the modal subspace and Masing's rule reconstructs the full modal hysteresis loop, assuming that the force-deflection hysteresis cycle is symmetric about the origin [25]. The nonlinear natural frequency and damping ratio can be calculated from this hysteresis curve as a function of α; see Eq. 12-17 in [21] for complete details. Figure 2 depicts the QSMA process and the utilization of Masing's Rule to generate a full and a quarter cycle from an initial quarter cycle.

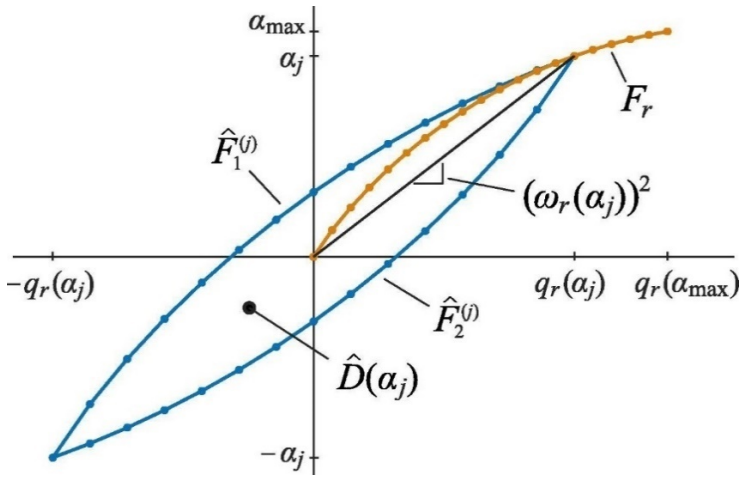

Figure 2: *A hysteresis curve generated using Masing's rule [21]*

3.0 FINITE ELEMENT MODEL OF MORPHING WING

This work applies the QSMA process on a finite element model of a finger-like mechanism morphing wing, as shown in Fig. 3. The goal is to evaluate the QSMA algorithm on a complex model with many contact interactions and degrees-of-freedom, to evaluate this approach for a realistic aerospace structure. The model is discretized with 510,819 fully integrated hexahedron elements. The adaptive wing subassembly is composed of many different parts consisting of five different materials. These materials and their corresponding properties are provided in Table 1. The ribs and links are aluminum, fixture and bolts are steel, and various washers are plastic. An exploded view of Block B1 is shown in Fig. 3. Unlike SARISTU [26], this single rib mechanism is coupled with a fixture designed to allow various configurations for experimental testing in place of using electromechanical actuation. For the purposes of this work, the structure is locked such that the chord line is parallel to ground.

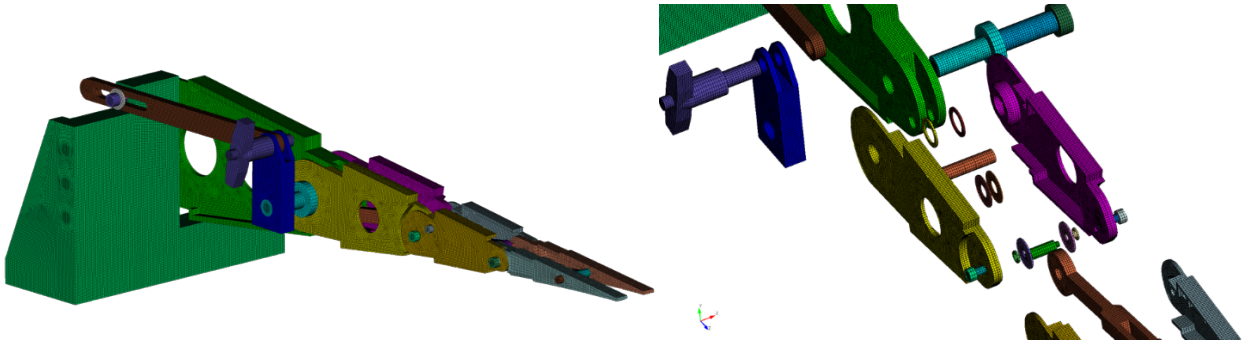

Figure 3: *(left) Finite element model of the morphing wing experimental structure, (right) Exploded view of section B1 depicting the internal components*

Table 1: *Material properties of morphing wing parts*

Material	Young's modulus (psi)	Density ($\frac{lb}{in^3}$)	Poisson's ratio	Coefficient of friction against Aluminum
6061-T6 Aluminum	1E7	0.0975	0.3	0.4
Alloy Steel	2.9E7	0.284	0.29	0.22
PFTE Plastic	1E5	0.0723	0.46	0.04
Acetal Plastic	4E5	0.0509	0.37	0.2
Stainless Steel	2.9E7	0.284	0.29	0.2

The full order finite element model consists of a total of 72 contact interfaces. To reduce the computational cost and complexity of the model, the interfaces were all considered and 33 of the interfaces were identified that are not expected to contribute significantly to energy dissipation through friction. These 33 interfaces were tied within the model using multipoint constraints. These surfaces included stiff interactions such as tightened bolts and rigid connections between the ribs. The remaining 39 contact interfaces include contacts between rib surfaces and hinge joints that allow the joints to rotate to a given wing shape during actuation. These nonlinear interfaces were modeled with Coulomb frictional contact elements with the assumed static friction coefficients listed in Table 1. Figure 4 depicts Block B2 with a rib moved to see the internal components, showing three types of joints: (1) bolted joints, (2) shoulder joints, and (3) pinned connections. All quasi-static contact simulations were conducted using implicit integration schemes using the Sierra Solid Mechanics [27] finite element solver. During flight, the joints in this morphing wing structure would be preloaded by the wing skin and by aerodynamic forces. In the laboratory tests that are planned with this prototype hardware, the joints would be preloaded via gravity loads or via a point load at the tip of the wing. This later case was simulated in the results presented in this paper.

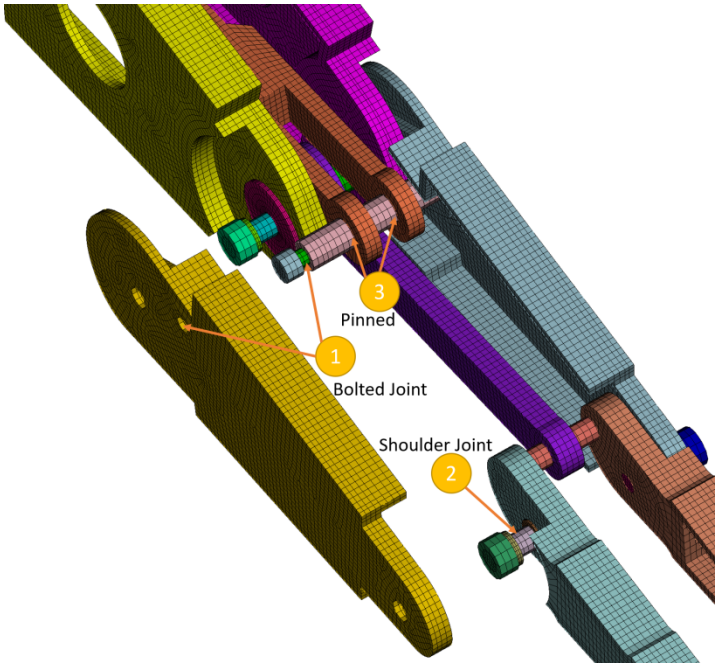

Figure 4: *Section B2 of the structure to show three types of joints*

To eliminate rigid body motion, the base of the fixture in Fig. 4 is constrained to have no displacement. Once the tip preload is applied and the contact solution converges, the solution can be used to determine which portions of each interface are in contact. These regions are then bonded to one another and linearized modal analysis is performed about the preloaded state for the next step in the QSMA process. The contact areas found in the preload step are also used to generate a Hurty/Craig-Bampton [28] model for the system as explained later.

4.0 FULL ORDER MODEL – PRELOAD

4.1 STATIC PRELOAD

The tip load used for the results presented in this work was given a magnitude of 3 lbf and distributed across four nodes at the tip of the structure. The peak tip displacement as a function of tip force is shown in Fig. 5. The load was incrementally ramped using a ramp-cosine function and then held steady for 100 timesteps to ensure that the equilibrium is accurately reached. The force-displacement curve reveals the nonlinear response of the wing structure due to the various frictional joints in the structure. Initially, the curve appears to exhibit softening behavior as the slope decreases. At a force level of around -0.3 lbf, there appears to be a sudden jump in response. Beyond this point, at higher load levels, the slope appears to increase with displacement suggesting a hardening behavior.

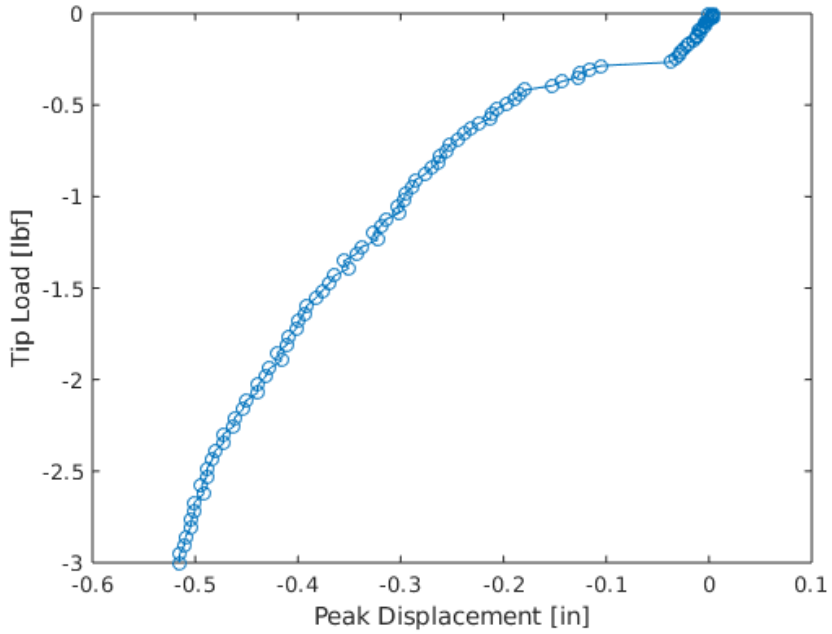

Figure 5: *Tip load versus peak displacement over the 100 preload steps*

The jump in displacement at about -0.3 lbf in Fig. 5 was investigated further and determined to be the result of a snap-through/buckling phenomenon during loading. Figure 6 show the axial stress in the link pin connecting blocks B2 and B3 before and after the event; these stress changes occurred over one load step increment. Prior to the snap-through, the pin was mostly in a compressive stress state. The sudden jump changed the stress state to a combined axial and bending stress, suggesting that the pin had buckled

under a combined compressive load and load applied from the link. Upon investigation of the model, this was the only quantity observed to change suddenly at these load levels, suggesting that this link was the source of the jump in displacement observed in the quasi-static loading curves. This buckling phenomenon is not thought to be physical, but an artifact of the model. A cause of this jump could be due to the coarse mesh of the hinge joints, leading to a phenomenon known as "facet locking" when rotating about a hinge joint. This highlights the challenges associated with detailed, nonlinear finite element analysis of complex mechanisms with many frictional contact interfaces throughout.

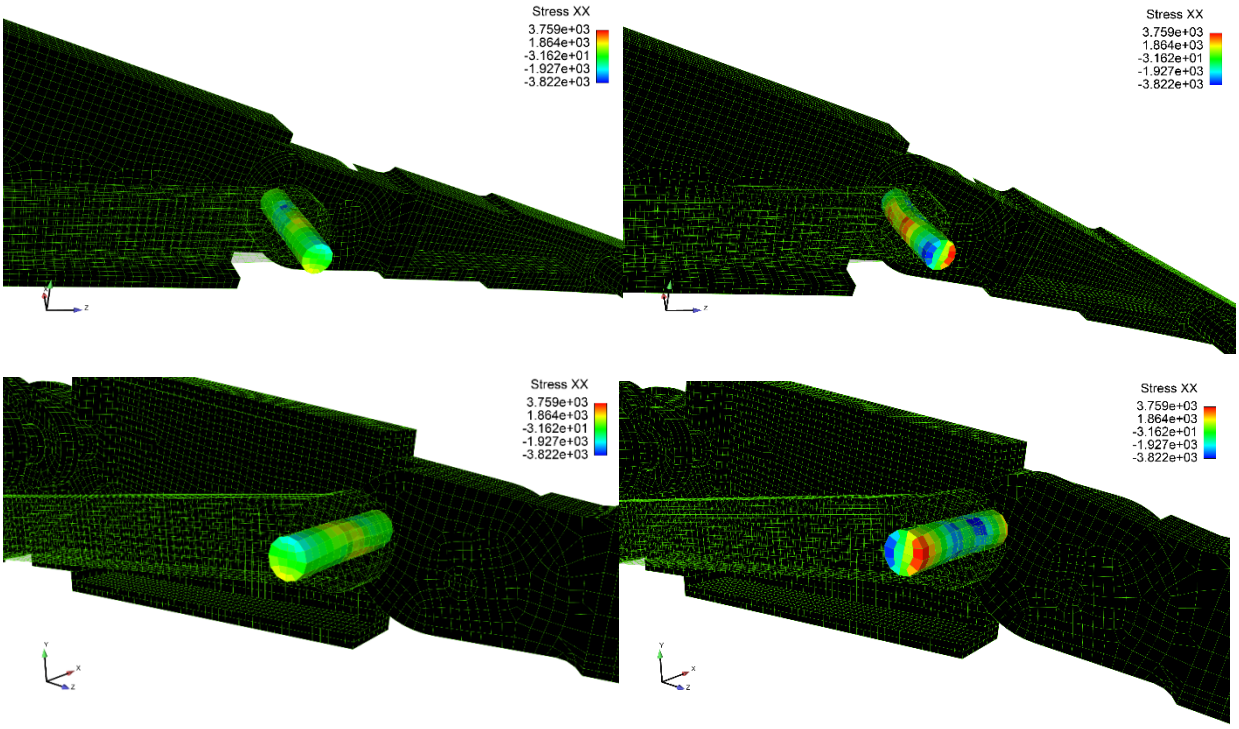

Figure 6: *Stress in* $[\boldsymbol{psi}]$ *before the snap-through on the back (row 1) and front (row 2) of the link connecting B2 and B3, (right) Stress after snap-through*

The contact statuses in all of the joints are shown in Fig. 7 for the instant when the tip preload is maximum. Some ribs have been removed to better visualize the internal components. A value of one (red) for contact status indicates the portion of the surface is in contact. A value of 0.5 (green) indicates that the surface was defined as a contact surface but is not computed to be in contact. Surfaces in blue are not defined as contact surfaces and thus are not in capable of supporting contact loads. Figure 8 provides a close up view of a shoulder joint, where the preload causes a portion of the hinge (red) to come into contact, while the opposite side (green) does not. The state of contact within the joints influence both the stiffness of the joint during the linearized modal analysis, as well as the energy dissipation of the joint during QSMA.

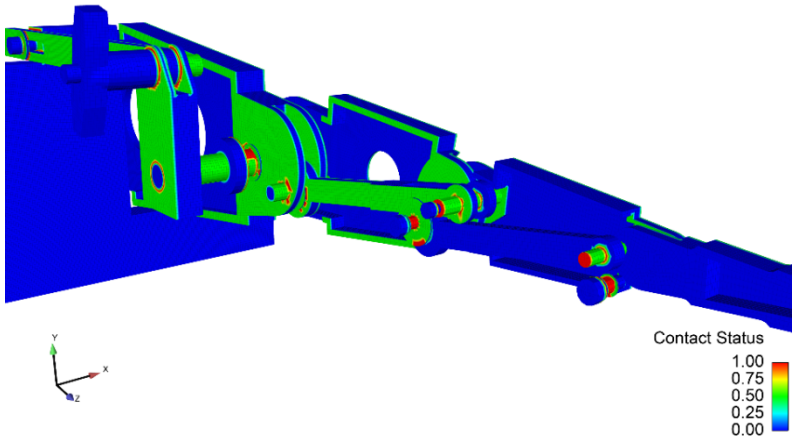

Figure 7: *The resulting contact status at the end of the preload simulation*

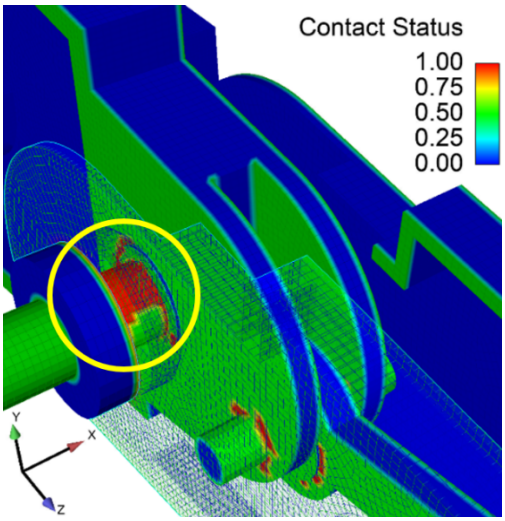

Figure 8: *Contact status of a joint where contact is allowed*

4.2 QUASI-STATIC MODAL ANALYSIS

Following the preload step, the next step in the QSMA process is to compute the linearized modes of vibration about the preloaded state. The modal analysis step was accomplished using the Sierra Structural Dynamic (Sierra/SD) [29] finite element code, which is able to import the deformation and stress state directly from the Sierra Solid Mechanics preload simulation. Within Sierra/SD, tied multipoint constraints can be defined based on the normal contact traction magnitudes calculated from the preload step. It should be noted that only fully tied interfaces were used within the modal analysis, i.e. the preloaded joints were constrained in both the normal and tangential directions. For the linearized modal analysis step, the chosen normal contact pressure cutoff value was 0 psi. Figure 9 depicts the mode of interest for the morphing wing structure, referred to as the first stiff direction bending mode, with a natural frequency of 166 Hz.

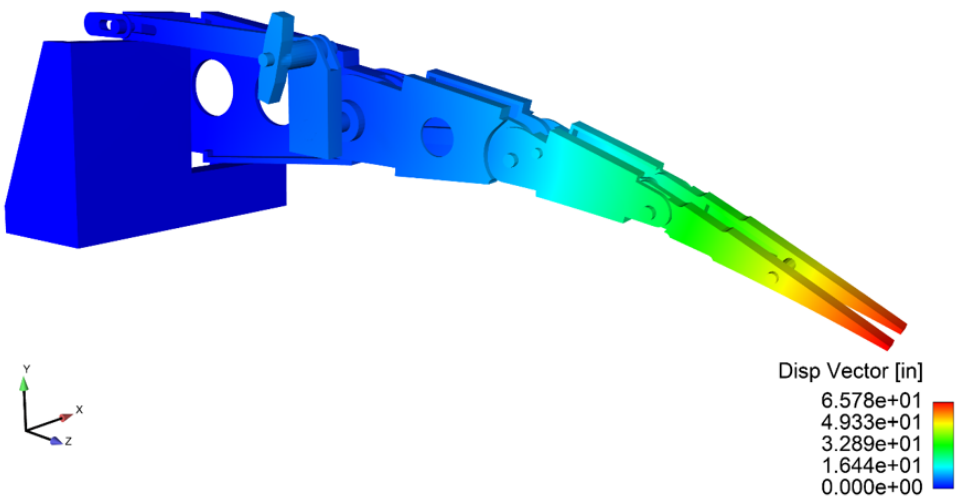

Figure 9: *Stiff bending mode of the morphing wing structure*

The final step of the QSMA process is to apply a body force to the structure proportional to the shape of the bending mode in Fig. 9. The modal force was applied to the structure such that the tip had a positive displacement, opposite of the tip preload step. The solver was allowed to settle for 50 additional iterations prior to applying the modal force to ensure that the model was in the equilibrium state.

After the modal filter was applied to the displacement fields, the nonlinear frequency and damping curves were computed and shown in Fig. 10. The modal force amplitude ranges were chosen such that the linearized model had a tip displacement in a prescribed range. In the results shown here, two separate simulations are shown for a tip displacement range of 0.005 to 0.05 inch, and 0.01 to 0.1 inch. The frequency and damping curves are plotted against the tip displacement (peak) quantify the relevant deflection in the mechanism when it vibrates in this mode. The two results appear to overlay each other quite well, suggesting that the method is repeatable for different forcing levels. The frequency curves in Fig. 10 show softening behavior as frequency initially decreases rapidly, and then appears to plateau to a lower value in the range of 60 to 70 Hz. The QSMA results should converge to the linearized frequency of 166 Hz at low displacement amplitudes, but this was not the case for the results shown here. This suggests that the smallest loads applied here were already large enough to cause a very significant frequency shift.

The damping is similarly computed from the load displacement data. The damping ratio curves shown in Fig. 10 achieved a peak value of almost 50% damping but decreased at higher displacement levels. Taken together, the QSMA curves appear to have the features of macro-slip behavior, where both the frequency and damping decrease after slip has initiated in the joints. Microslip behavior typically shows increasing damping ratios with displacement level, and slight decreases in the natural frequency as small regions of the joint begin to slip.

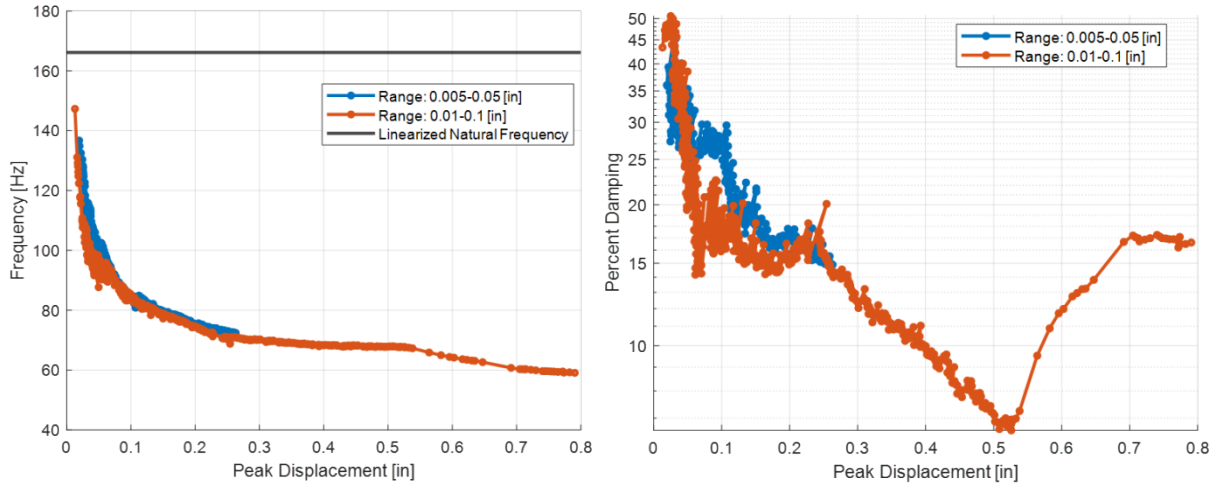

Figure 10: *Frequency (left) and damping (right) as a function of displacement amplitude estimated using QSMA*

It was observed that the peak tip displacement resulting from the modal force was much greater than the prescribed tip displacement from the linearized analysis, up to eight times the prescribed level. These results suggest that even the lowest loads applied were causing significant slip in the joints, more than would be expected for the linearized model where the preloaded interfaces were assumed to be fully tied (or stuck). Efforts were made to apply even lower force amplitudes with the QSMA approach; however, the implicit solver was unable to converge and produce reasonable results. When the magnitude of the modal force was small relative to the preload force, the response to the preload seemed to dominate, hence resulting in a noisy response to the modal force and unreasonable results with QSMA.

There are several assumptions that were made that could be questioned at this point. Error could arise from the mesh discretization within the frictional interfaces. Considering that the contact happens on cylindrical surfaces, the model likely needs more refinement in the area of the hinge joints in order to properly capture the contact and slip. However, the model already has over 500K elements. This highlights a key challenge for the analysis of jointed structures; the physics of interest may require extreme levels of refinement locally, far more than is typically needed for accurate stress analysis or to predict the natural frequencies well. Another assumption of the QSMA approach is that the joints obey Masing's hypothesis such that the hysteresis curves can computed from the initial loading curve. If this assumption is not satisfied, one must compute the full hysteresis curve quasi-statically. This hypothesis can be directly evaluated by computing the modal hysteresis curve for the mode of interest and comparing it directly to the hysteresis curve reconstructed using Masing's rule. To do this, the modal force was applied to the structure in a forward cycle discretized from 0 → α → -α → α, as well as a reverse cycle discretized from 0 → -α → α → -α. The resulting modal hysteresis curves are shown in Fig. 11.

The first observation from these data are that the hysteresis curves are different for the forward and reverse loading cycles. Additional loading cycles would be needed to reach steady-state and close the hysteresis loops, indicating either that the computational model is not realistic or that the behavior of the structure is far more complicated than expected. To explore this further, in Fig. 12 the reverse loading cycle is compared to hysteresis loop generated from the initial quarter cycle of the reverse load using Masing's rules.

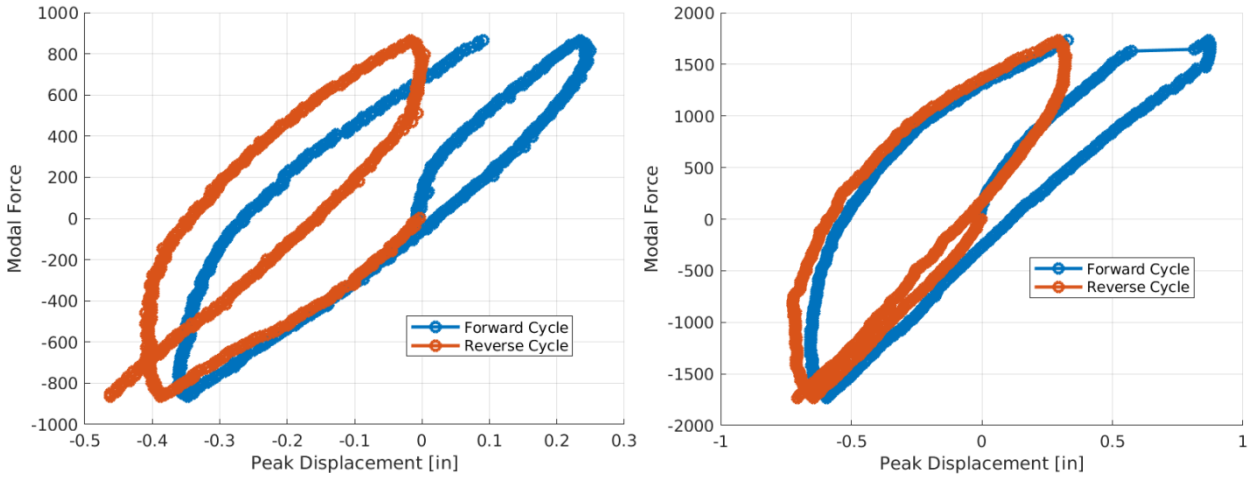

Figure 11: *Moderate (Left), High (Right) modal force vs. peak displacement hysteresis loop*

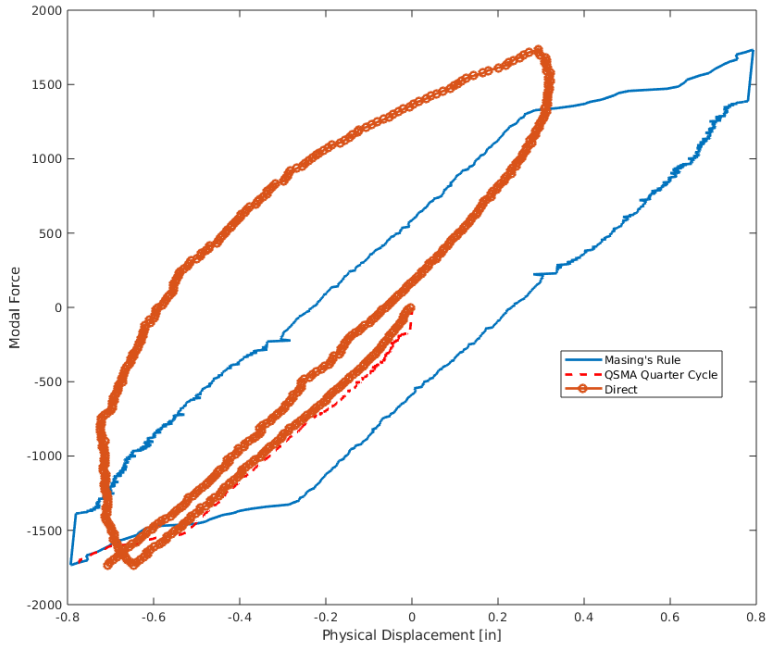

Figure 12: *QSMA vs. direct static hysteresis loop for the modal force step*

The two results are quite different in terms of shape (i.e. stiffness) and the area enclosed (damping). Although the quarter cycle initially follows the direct hysteresis loop, it deviates at higher displacements. At this point it is unclear whether these results are reliable or not. It has been shown that if the contact pressure varies over a loading cycle then a model with Coulomb friction can violate Masing's rules [21], and considering the low preload in these joints, this could be the case here. Conversely, the physics observed could be spurious and due to an inadequate mesh in the contact regions. While this case study cannot resolve these issues, it does raise some important issues that one must be aware of when applying QSMA to a complex structure.

4.3 REDUCED ORDER MODEL

In addition to the full-order model, a reduced order model (ROM) of the morphing wing structure was developed using the whole joint approach [22]. The ROM was derived from the full-order model using the following process. First, contact surfaces at the joints are defined within the full-order model and a preload analysis was performed to determine the contact status of all contact interfaces. From the preload results, a subset of each contact surface was defined to include only the nodes/faces on the surface in contact. This subset of each interface was then assigned to a multipoint constraint, or "spider", to tie all these nodes on the surface to a single, virtual node using either averaging or rigid bar elements. Next, two spider joints at a contact interface were connected by a whole joint model in between the virtual nodes, each whole joint having six independent DOF. The joints can be assigned any constitutive element to represent the physics of interest. In this study, the model contains linear spring elements whose stiffness may be easily altered to approximate the stiffness of the contact interface. This spidering method, as shown schematically in Fig. 13, was performed on all hinged joint and frictional contact interfaces in the morphing wing model.

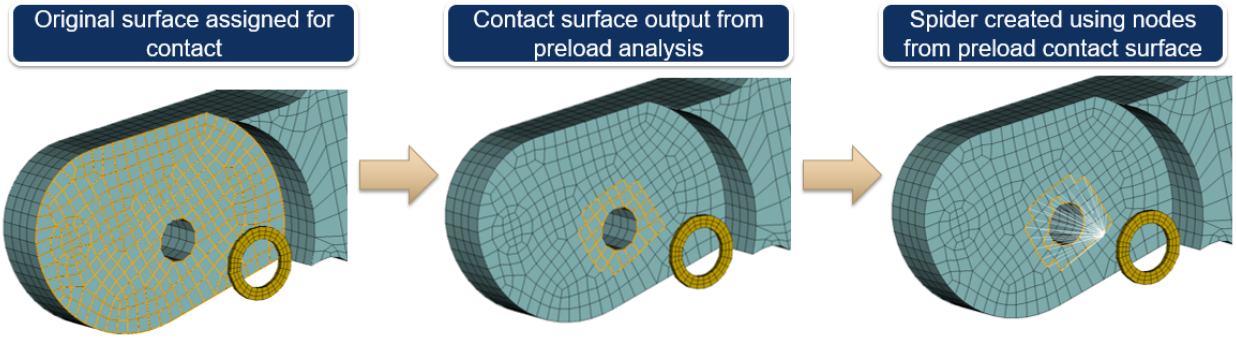

Figure 13. *Spidering process example for a rib-to-washer contact interface*

There is no way to predict the stiffness that a whole joint model such as this should have, and so some sort of optimization was needed. Towards this end, a rotational stiffness sensitivity study was conducted on the morphing wing subassembly. The rotational stiffness about the x-axis, denoted as KRx, which is the same for all the hinged joints in the current model, was varied from 1e1 to 1e9 in-lbf while all other stiffnesses (rotational and axial) were held constant at 1+E08 in-lbf or lbf/in, depending on whether it is a rotational or translational DOF. Modal analysis was performed on the reduced order model at each KRx stiffness value to determine how the frequency of the mode of interest changes. The 2nd mode natural frequency was found to vary significantly with changing rotational stiffness, as shown in Fig. 13. At low stiffness values, the mode converges to around 50 Hz. As the rotational stiffness increases, the frequency increases and converges to an upper bound of around 110 Hz. The lower bound on the mode frequency is within the range of the lower frequency bound of the QSMA results in Fig. 10. This lower bound would correspond to the response when the joint has slipped, and no rotational stiffness is provided by the joint. The upper bound was smaller than the mode frequency with all joints stuck, and so presumably this spring would need to be set in conjunction with others to cause the model to agree with the linear eigenvalue results.

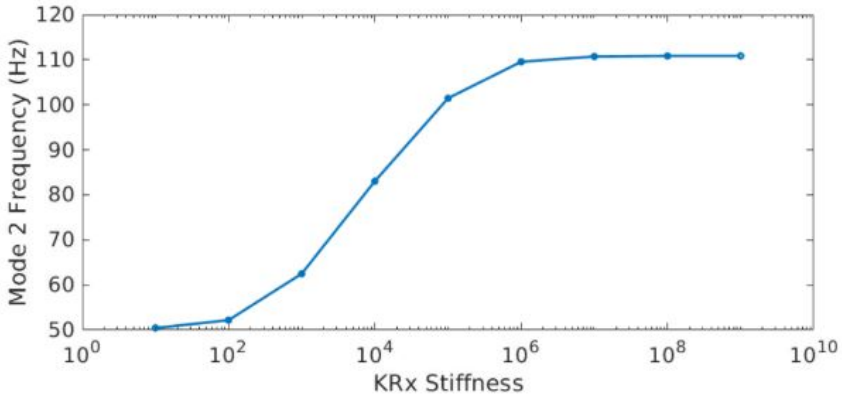

Figure 13: *Mode 2 frequency with increasing rotational stiffness, KRx*

5.0 CONCLUSIONS AND FUTURE WORK

High fidelity nonlinear finite element models can provide new insights to guide the design and predict the performance of complex aerospace structures, yet those models can be extremely expensive to simulate and this severely limits our ability to understand their dynamics. This work utilized the QSMA framework to study an industrial scale structure of a morphing wing and provided a preliminary view of how this algorithm may scale to a large-scale model. The amplitude dependent natural frequency and damping ratio curves from the full order model were found to show significant loss of stiffness in the joint, as well as significant levels of energy dissipation, even when the structure responds at lower amplitudes for the mode of interest. The QSMA results were investigated by directly calculating the modal hysteresis curves, and the results suggested that the mode under study violated Masing's hypothesis since the reconstructed hysteresis loop did not overlay with the directly computed curves. This seems to be a valuable check of the validity of QSMA for complex structures. The results to date are promising but show that more effort is needed to scale the methodology to general large-order structural models. One potential area requiring further attention is the mesh density at the localized regions of the joint; for this method to be practical on very large models it seems that one needs a convenient way to increase the mesh resolution in very small regions near interfaces.

The present study was only able to initiate a reduced order model for this system, but there was not sufficient time to determine whether the ROM could be tuned to agree with the full order model for the modes of interest. In future studies the authors hope to explore this and better quantify the advantages and disadvantages of using spiders in this framework to model a structure. Additionally, experimental data should be acquired to supplement the modeling work to provide validation data as well as provide key insights into the modelling assumptions used throughout this study.

ACKNOWLEDGMENTS

This research was conducted at the 2020 Nonlinear Mechanics and Dynamics (NOMAD) Research Institute supported by Sandia National Laboratories in partnership with the University of New Mexico. Sandia

National Laboratories is a multimission laboratory managed and operated by National Technology and Engineering Solutions of Sandia, LLC., a wholly owned subsidiary of Honeywell International, Inc., for the U.S. Department of Energy's National Nuclear Security Administration under contract DE-NA-0003525. The authors would also like to thank Jack Heister and Rick Garcia from Sandia National Laboratories for their support in the design and mesh creation of the morphing wing device presented throughout this work.

REFERENCES

[1] R. Pecora, A. Concillo, I. Dimino, F. Amoroso, and M. Ciminello, "Structural design of an adaptive wing trailing edge for enhanced cruise performance," presented at the 24th AIAA/AHS Adaptive Structures Conference, San Diego, CA, 2016.

[2] I. Dimino, A. Concilio, and R. Pecora, "An Adaptive Control System for Wing TE Shape Control," presented at the SPIE International Conference on Smart Structures, San Diego, CA, 2013.

[3] R. Pecora, F. Amoroso, M. C. Noviello, I. Dimino, and A. Concilio, "Aeroelastic stability analysis of a large civil aircraft equipped with morphing winglets and adaptive flap tabs," Mar. 2018, vol. 10595, doi: 10.1117/12.2300173.

[4] K. L. Bonnema, "AFTI/F-111 Mission Adaptive Wing Briefing to Industry," AFWAL Technical Report, Oct. 1988.

[5] L. D. Webb, W. E. McCain, and I. A. Rose, "Measured and Predicted Pressure Distributions on the AFTI-F-111 Mission Adaptive Wing," in *NASA Technical Memorandum TM-100443, National Aeronautics and Space Administration*, Edwards, Ed. 1988.

[6] R. Calzada and N.A.S.A., Apr. 17, 1998, [Online]. Available: https://www.nasa.gov/centers/dryden/multimedia/imagegallery/F-111AFTI/F-111AFTI_proj_desc.html.

[7] N.A.S.A., *Past Project: Adaptive Compliant Trailing Edge Flight Experiment*. 2014.

[8] O. Bilgen, K. B. Kochersberger, D. J. Inman, and O. J. Ohanian, "Novel, Bidirectional, Variable-Camber Airfoil via Macro-Fiber Composite Actuators," *Journal of Aircraft*, vol. 47, no. 1, pp. 303–314, Jan. 2010, doi: 10.2514/1.45452.

[9] A. D. Gaspari, L. Riccobene, and S. Ricci, "Design, manufacturing and wind tunnel validation of a morphing compliant wing," *Journal of Aircraft*, vol. 55, no. 6, 2018.

[10] A. Wildschek *et al.*, "Multi-Functional Morphing Trailing Edge for Control of All-Composite, All-Electric Flying Wing Aircraft," in *The 26th Congress of ICAS and 8th AIAA ATIO*, American Institute of Aeronautics and Astronautics.

[11] P. D. Vecchia, S. Corcione, R. Pecora, F. Nicolosi, I. Dimino, and A. Concilio, "Design and integration sensitivity of a morphing wing trailing edge on a reference airfoil: The effect on high-altitude long-endurance aircraft performance," *Journal of Intelligent Material Systems and Structures*, 2017.

[12] R. Pecora, F. Amoroso, and L. Lecce, "Effectiveness of wing twist morphing in roll control," *Journal of Aircraft*, vol. 49, no. 6, pp. 1666–1674, 2012.

[13] R. Pecora *et al.*, "Actuator Device Based on a Shape Memory Alloy, and a Wind Flap Assembly fitted with such an Actuator Device"," in *United States Patent US 8348201*, 2018.

[14] I. Dimino, G. Amendola, R. Pecora, A. Concilio, A. Gratias, and M. Schueller, "Chapter 22 - On the Experimental Characterization of Morphing Structures," in *Morphing Wing Technologies*, A. Concilio, I. Dimino, L. Lecce, and R. Pecora, Eds. Butterworth-Heinemann, 2018, pp. 683–712.

[15] S. Kuzmina *et al.*, "Chapter 23 - Wind Tunnel Testing of Adaptive Wing Structures," in *Morphing Wing Technologies*, A. Concilio, I. Dimino, L. Lecce, and R. Pecora, Eds. Butterworth-Heinemann, 2018, pp. 713–755.

[16] O. Schorsch, A. Lühring, and C. Nagel, “Elastomer-Based Skin for Seamless Morphing of Adaptive Wings,” in *Smart Intelligent Aircraft Structures (SARISTU)*, Cham, 2016, pp. 187–197.
[17] G. Amendola, I. Dimino, R. Pecora, A. Concilio, and F. Amoroso, “Preliminary design of an adaptive aileron for the next generation regional aircraft,” *Journal of Theoretical and Applied Mechanics*, vol. 55, pp. 307–316, 2017.
[18] G. Amendola, I. Dimino, A. Concilio, M. Magnifico, and R. Pecora, “Numerical design of an adaptive aileron,” Las Vegas, NV, Mar. 2016.
[19] G. Amendola, I. Dimino, F. Amoroso, and R. Pecora, “Experimental characterization of an adaptive aileron: Lab tests and FE correlation,” Las Vegas, NV, 2016.
[20] R. Pecora, F. Amoroso, M. Magnifico, I. Dimino, and A. Concilio, “KRISTINA: Kinematic rib-based structural system for innovative adaptive trailing edge,” in *Industrial and Commercial Applications of Smart Structures Technologies 2016*, Apr. 2016, vol. 9801, p. 980107, doi: 10.1117/12.2218516.
[21] R. M. Lacayo and M. S. Allen, “Updating Structural Models Containing Nonlinear Iwan Joints Using Quasi-Static Modal Analysis,” *Mechanical Systems and Signal Processing*, vol. 118, no. 1 March 2019, Art. no. 1 March 2019, 2019.
[22] D. J. Segalman, “Modelling joint friction in structural dynamics,” *Structural Control and Health Monitoring*, vol. 13, no. 1, Art. no. 1, Jan. 2006, doi: 10.1002/stc.119.
[23] E. Jewell, M. S. Allen, I. Zare, and M. Wall, “Application of Quasi-Static Modal Analysis to a Finite Element Model and Experimental Correlation,” *Journal of Sound and Vibration*, vol. 479, no. 4 August, Art. no. 4 August, 2020.
[24] H. Festjens, G. Chevallier, and J.-L. Dion, “A numerical tool for the design of assembled structures under dynamic loads,” *International Journal of Mechanical Sciences*, vol. 75, pp. 170–177, 2013, doi: 10.1016/j.ijmecsci.2013.06.013.
[25] G. Masing, “Eigenspannungen und verfestigung beim messing (self stretching and hardening for brass),” 1926, pp. 332–335.
[26] C. I. R. A.-. CIRA, “SARISTU Project Adaptive Wing.” [Online]. Available: http://futuroremoto.cira.it/saristu_eng.html.
[27] SIERRA Solid Mechanics Team, “Sierra/SolidMechanics 4.56.2 User’s Guide,” Sandia National Laboratories, Albuquerque, NM, SAND2020-5362, May 2020.
[28] W. C. Hurty, “Dynamic analysis of structural systems using component modes,” *AIAA Journal*, vol. 3, no. 4, Art. no. 4, Apr. 1965, doi: 10.2514/3.2947.
[29] Sierra Structural Dynamics Development Team, “Sierra/SD – User’s Manual – 4.56,” Sandia National Laboratories, Albuquerque, NM, SAND2020-3028, Apr. 2020.